Journal of Environmental Management 353 (2024) 120114

Contents lists available at ScienceDirect

Journal of Environmental Management

journal homepage: www.elsevier.com/locate/jenvman

Research article

Co-immobilizing laccase-mediator system by *in-situ* synthesis of MOF in PVA hydrogels for enhanced laccase stability and dye decolorization efficiency

Xue Yang [a], Xinyi Chen [a], Hongbo Wang [a], Artur Cavaco-Paulo [a,b], Jing Su [a,*]

[a] Jiangsu Engineering Technology Research Centre of Functional Textiles, Jiangnan University, Wuxi, 214122, China
[b] Centre of Biological Engineering, University of Minho, Campus de Gualtar, 4710-057, Braga, Portugal

ARTICLE INFO

Handling Editor: Lixiao Zhang

Keywords:
Co-immobilized laccase-mediator
Metal-organic frameworks
Water remediation

ABSTRACT

The laccase mediator system (LMS) with a broad substrate range has attracted much attention as an efficient approach for water remediation. However, the practical application of LMS is limited due to their high solubility, poor stability and low reusability. Herein, the bimetallic Cu/ZIFs encapsulated laccase was *in-situ* grown in poly (vinyl alcohol) (PVA) polymer matrix. The PVA-Lac@Cu/ZIFs hydrogel was formed via one freeze-thawing cycle, and its catalytic stability was significantly improved. The mediator was further co-immobilized on the hydrogel, and this hierarchically co-immobilized ABTS/PVA-Lac@Cu/ZIFs hydrogel could avoid the continuous oxidation reaction between laccase and redox mediators. The co-immobilized LMS biocatalyst was used to degrade malachite green (MG), and the degradation rate was up to 100 % within 4 h. More importantly, the LMS could be recycled synchronously from the dye solutions and reused to degrade MG multiple times. The degradation rate remained above 69.4 % after five cycles. Furthermore, the intermediate products were detected via liquid chromatography-mass spectrometry, and the potential degradation pathways were proposed. This study demonstrated the significant potential of utilizing the MOF nanocrystals and hydrogel as a carrier for co-immobilized LMS, and the effective reuse of both laccase and mediator was promising for laccase application in wastewater treatment.

1. Introduction

Laccases are one type of multicopper-containing oxidases with high catalytic efficiency and less by-product for bioremediation, which exhibit excellent competence towards sustainable water treatment processes (Dong et al., 2023; Su et al., 2018; Zhou et al., 2021). Combining the redox mediators as a laccase-mediator system (LMS) is mainly involved in hydroxylation, carbon-carbon bond cleavage and carbonylation, which is added further to broaden the range of catalyzed substrates for laccase (Cañas and Camarero, 2010; Luo et al., 2018; Yao et al., 2022). For the industrialized application of enzymes, the co-immobilization of redox mediators and laccase has been extensively investigated in recent years to realize the synchronous recycling of LMS and enhance their catalytic stability (Hwang and Lee, 2019; Zdarta et al., 2021; Zhang and Hay, 2020).

Recently, metal-organic frameworks (MOFs) are organic-inorganic hybrid crystalline coordination polymers demonstrated as advantageous carriers for enzyme immobilization (Drout et al., 2019; Li et al., 2022b; Liang et al., 2021b). Moreover, the MOFs with high stability, tunable pore size and large pore volume could protect the enzyme from harsh environments and further allow the substrates to diffuse in active sites of laccase (Chandio et al., 2024; Hu et al., 2018). Zhang et al. encapsulated the laccase in Cu-MOFs via the one-pot method, and the immobilized laccase showed excellent stability (Zhang et al., 2020). Furthermore, the degradation rate of laccase@Cu-MOFs for bisphenol A reached 100 % within 4 h. Hsu et al. successfully prepared the zinc-based metal-organic framework using a de novo mild water-based system at room temperature, and the catalase enzyme was encapsulated into Zn-MOF-74 (Hsu et al., 2021). Unfortunately, the MOF crystalline powders were easily broken down in the mobile phase and difficult to recover in practical applications, causing heavy losses and poor reusability (Liu et al., 2022; Zhao et al., 2021). A hydrogel with plenty of crosslinked polymer chains has been regarded as the ideal material to incorporate porous MOFs to construct soft/hard-coupled

* Corresponding author.
E-mail address: sujing@jiangnan.edu.cn (J. Su).

https://doi.org/10.1016/j.jenvman.2024.120114
Received 4 December 2023; Received in revised form 11 January 2024; Accepted 12 January 2024
Available online 26 January 2024

structures (Ahmadian et al., 2023; Wang et al., 2019; Wu et al., 2023). Poly(vinyl alcohol) (PVA) is a versatile non-ionic hydrophilic polymer that has drawn much attention because of its nontoxicity, mechanical stability, and biocompatibility (Liu et al., 2023; Luo et al., 2021). In addition, it is a biodegradable, water-soluble, cost-effective, thermoplastic and environmentally friendly polymeric material with good chemical stability (Duman et al., 2022a, 2022b, 2022c). More importantly, the gelation occurred and formed PVA hydrogels via a simple freeze-thawing cycles method without using crosslinking agents. Peng et al. prepared different pre-synthesized MOFs/PVA to immobilize laccase, and PVA-based hydrogels were formed through five freeze-thawing cycles (Peng et al., 2021). Wang et al. developed a Janus hydrogel tape with single-sided adhesiveness by three cyclic freezing-thawing (−18 °C, 12 h/room temperature, 12 h) (Wang et al., 2022a). Hu et al. proposed that a PVA-based conductive hydrogel was fabricated via three freezing-thawing processes (−20 °C, 12 h/room temperature, 6 h) (Hu et al., 2022). Although the immobilized laccase exhibits stability and reusability, the preparation process is complicated and usually needs a long freeze-thawing time. Hence, exploring a facile and generalizable method for preparing MOF/hydrogel composites is essential for further immobilized laccase. In addition, further exploration was needed to utilize the MOF/hydrogels composites to achieve the hierarchical immobilization of laccase and redox mediators.

Herein, we report a method to co-immobilize laccase and redox mediators hierarchically with MOF/hydrogel composites for water treatment. This hierarchical co-immobilization method could prevent the continuous oxidation reaction between laccase and redox mediators during the simultaneous immobilization process. Moreover, compared with other gelation processes that usually require several cycles, only one freeze-thawing cycle (−20 °C, 12 h/25 °C, 2 h) was needed to fabricate MOF/hydrogel. The laccase was encapsulated into bimetallic Cu/ZIFs and then anchored into PVA hydrogel. The morphology, chemical structure, mechanical property and enzyme properties of PVA-Lac@Cu-ZIFs hydrogel were further characterized. After that, the redox mediator 2,2-azino-bis-3-ethylbenzothiazoline-6-sulfonic acid (ABTS) was immobilized on the hydrogel (PVA/ABTS-Lac@Cu-ZIFs). Malachite green, a typical triphenylmethane dye, was used to simulate the textile wastewater to demonstrate further the potential of PVA/ABTS-Lac@Cu-ZIFs hydrogel in wastewater treatment. Furthermore, the enzymatic reaction mechanisms and degradation pathway were investigated.

2. Experimental

2.1. Materials

Laccase (0.5 U/g) from Trametes versicolor was purchased from Sigma-Aldrich. (St. Louis, MO, USA). Zinc nitrate hexahydrate, copper (II) nitrate hydrate, poly(vinyl alcohol) (PVA; polymerization degree is 1700, hydrolysis degree is 99 %), sodium chloride (NaCl), potassium chloride (KCl), calcium chloride ($CaCl_2$), congo red (CR), reactive blue 19 (RB) and malachite green (MG) were supplied by from Sinopharm Chemical. Imidazole-2-carboxaldehyde (ICA), acid Orange 7 (AO), polyvinyl pyrrolidone (PVP Mw = 40,000), and 2, 2′-azino-bis (3-ethylbenzothiazoline-6-sulfonic acid) (ABTS) (≥99.0 %), were acquired from InnoChem Science & Technology. (Beijing, China).

2.2. Synthesis of PVA-Lac hydrogel

10 g of poly(vinyl alcohol) (PVA) was added into 40 mL deionized (DI) water at 95 °C for 3 h with mechanical stirring and then cooled to 35 °C. The laccase powders (300 mg) were dissolved into 10 mL DI water. The mixture was placed into a flask and stirred at 35 °C for 10 min. Then, the solution was poured into polystyrene dishes after degassing via sonication and put in the refrigerator (−20 °C) for 12 h. The PVA-Lac biocomposite was obtained by thawing at room temperature for 2 h. For structural analysis, the PVA-Lac was subjected to vacuum-free drying.

2.3. Synthesis of PVA-Lac@Cu/ZIFs hydrogel

PVA (10 g) and imidazole-2-carboxaldehyde (ICA) (500 mg) were dissolved in 39.5 mL DI water at 95 °C for 3 h with mechanical stirring and then cooled to 35 °C. Then, the $Zn(NO_3)_2{\cdot}6H_2O$ (241.6 mg) and $Cu(NO_3)_2{\cdot}3H_2O$ (892.5 mg) were added in 10 mL DI water, and polyvinyl pyrrolidone (PVP) (50 mg) and laccase powders (300 mg) were added with constant stirring for 5 min. These two solutions were mixed and stirred at 35 °C for 10 min. Then, the solution was poured into polystyrene dishes after degassing via sonication and put in the refrigerator (−20 °C) for 12 h. The PVA-Lac@Cu/ZIFs biocomposite was obtained by thawing at room temperature for 2 h. For structural analysis, the biocomposite was subjected to vacuum-free drying.

2.4. Preparation of co-immobilized laccase and ABTS hydrogel

The PVA-Lac and PVA-Lac@Cu/ZIFs hydrogels were put into the ABTS aqueous solution and shaken at 150 rpm (6 h, 35 °C) to immobilize ABTS molecules onto the hydrogel. The effect of ABTS dosage (1–8 mmol) on immobilization was investigated, and the optimal immobilization conditions were determined by ABTS loading and degradation efficiency for MG. The ABTS was oxidized to $ABTS^{\cdot+}$ using potassium persulfate and was determined with the direct spectrophotometric method 732 nm. The calibration curves for determining $ABTS^{\cdot+}$ were shown in Fig. S1.

2.5. Materials characterization and measurements

The materials characterization and measurements are provided in **Supplementary Information**.

3. Results and discussion

3.1. Fabrication and characterization of PVA-Lac and PVA-Lac@Cu-ZIFs hydrogel

Fig. 1 schematically showed the preparation process of PVA-Lac@Cu-ZIFs hydrogel, which was indicated by the purple arrows. The PVA and organic ligands (ICA) solution was first fully dissolved in DI water. The Zn^{2+} and Cu^{2+} were added to polymer chains, and *in-situ* synthesized the MOFs nanocrystals. Meanwhile, the free laccase was encapsulated into the bimetal MOF nanocrystals. Finally, one freeze-thawing cycle (−20 °C, 12 h/25 °C, 2 h) was proceeded for preparing the PVA-Lac@Cu-ZIFs hydrogel. The ice crystals between the polymers were formed and drove the realignment of polymer chains, which would serve as crosslinks. Therefore, the polymer chains and MOF nanocrystals were prepacked microscopically to form aggregation (Wu et al., 2017). The water molecules were discharged from the PVA chains during the melting process, which promoted the formation of hydrogen bonds between the hydroxyls (Chen et al., 2023). Meanwhile, the aggregation and crystallization of polymer chains further formed a crystalline region. (Fig. 1b). Besides the PVA with active hydroxyl groups interacting with ICA, the organic ligands monomer was adsorbed on the PVA surface. As the metal ions doped, the diverse hierarchical pores of MOF nanocrystals were *in-situ* synthesized and crosslinked with plentiful polymer chains. The morphologies of the Cu-ZIF-90 were observed via FESEM and shown in Fig. 1c. The characteristic of Cu-ZIF-90 exhibited flower-like structures consistent with our previous work (Yang et al., 2023). Furthermore, the FESEM image of the freeze-dried PVA-Lac@Cu-ZIFs hydrogel sample displayed the rough surface (Fig. 1d). The Cu-ZIF-90 nanocrystals were *in-situ* growth on the PVA polymer chains and interacted between the polar character of Cu-ZIF-90 and hydrophilic polymers, the appearance of protrusions on the surface was increasing accordingly, implying the formation of the MOF agglomeration in the polymer matrix

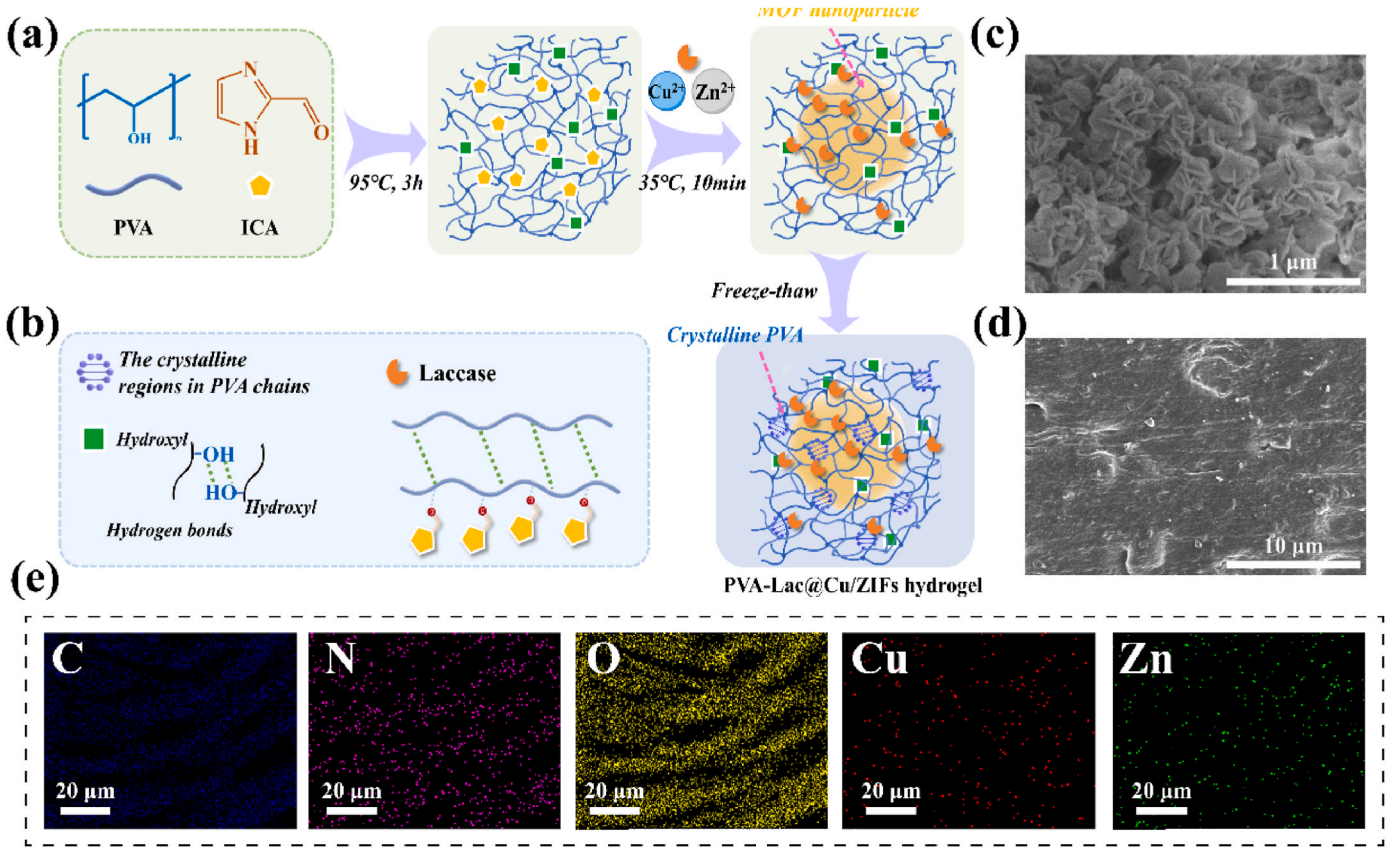

Fig. 1. (a) Schematic illustrations for synthesizing the PVA-Lac@Cu-ZIFs hydrogel. (b) The crystalline region and hydrogen bonds in hydrogels. FESEM images of Cu/ZIF-90 (c) and PVA-Lac@Cu-ZIFs (d). EDS elemental mapping of PVA-Lac@Cu-ZIFs (e).

(Rahman et al., 2023). The distribution of Cu-ZIF-90 in PVA hydrogel was further analyzed via EDS spectra, as shown in Fig. 1e. The EDS mapping images of PVA-Lac@Cu-ZIFs hydrogel clearly showed a uniform distribution of C, N, O, Cu and Zn elements.

An investigation with XRD was carried out to understand the PVA-Lac@Cu/ZIFs hydrogels properties. As shown in Fig. S3, the XRD

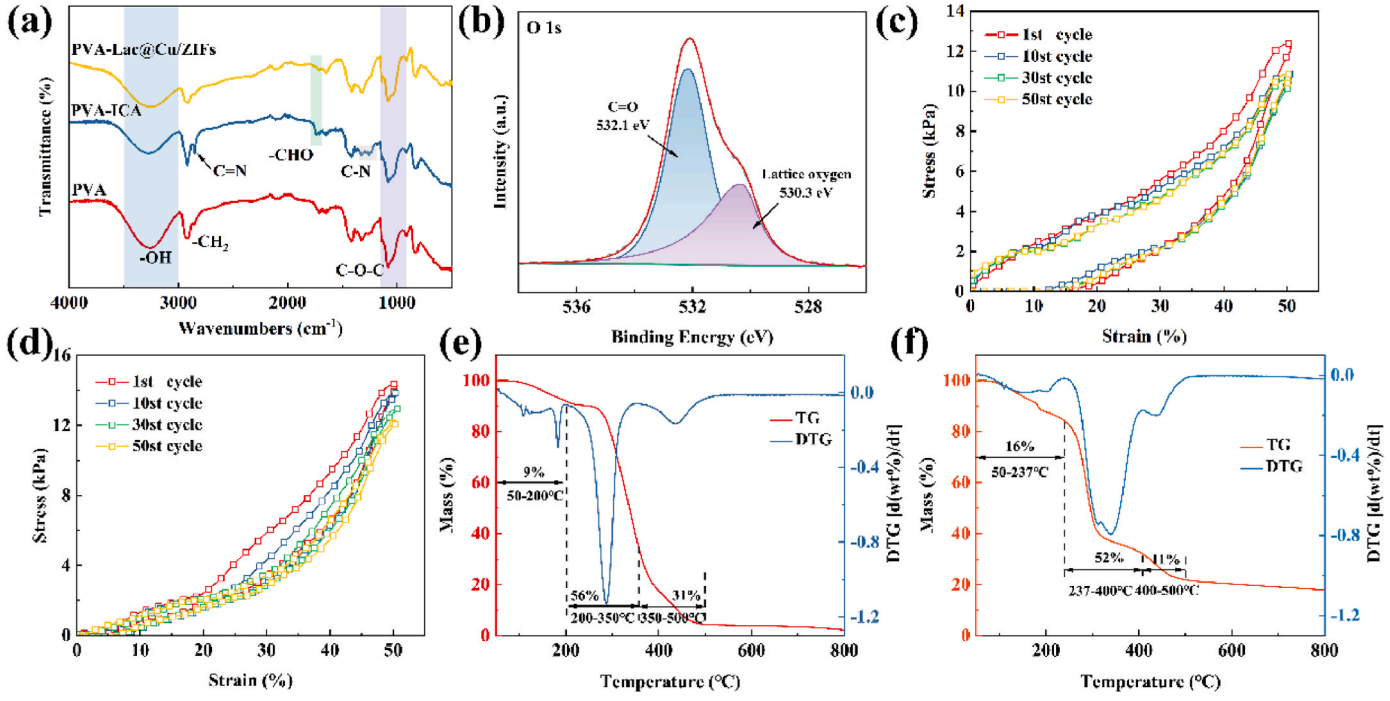

Fig. 2. (a) FTIR spectra of PVA, PVA-ICA and PVA-Lac@Cu/ZIFs. (b) Typical high-resolution O 1s of PVA-Lac@Cu/ZIFs. Stress-strain curves of compression–relaxation cycle for PVA-Lac (c) and PVA-Lac@Cu/ZIFs (d) hydrogel. TG and DTG curves of PVA-Lac (e) and PVA-Lac@Cu/ZIFs (f) hydrogel.

pattern of Cu/ZIFs showed significant peaks at 13.1° and 16.2°. The XRD patterns of PVA-Lac@Cu/ZIFs exhibited the main characteristic peaks of Cu/ZIFs, demonstrating the successful anchoring of MOFs on the PVA polymer matrix. Based on the FTIR spectra of PVA-ICA and PVA-Lac@Cu/ZIFs (Fig. 2a), the –CHO groups belonged to the ligand of MOFs, confirmed that the MOFs have been synthesized in the hydrogels (Dai et al., 2022). Furthermore, the O 1s spectrum of PVA-Lac@Cu/ZIFs showed two peaks at 530.3 and 532.1 eV (Fig. 2b), corresponding to the lattice oxygen and C═O, respectively (Dai et al., 2023; Idriss, 2021). This result demonstrated that the interaction between metal and oxygen atoms in the MOFs further confirmed the synthesis of MOFs. Furthermore, the ICP-MS additionally exhibited that the loading efficiency of Cu and Zn in PVA hydrogel was around 0.47 % and 1.63 %, respectively.

Repeated compressive tests evaluated the compression performance and recoverability of PVA-Lac and PVA-Lac@Cu/ZIFs. As shown in Fig. 2 (c - d), the *in-situ* growth of MOFs anchoring onto PVA hydrogel could provide structural stability. The hydrogels were compressed at 50 % strain, and the compression-relaxation cycles were repeated fifty times. The stress of PVA-Lac and PVA-Lac@Cu/ZIFs hydrogel were 12.3 kPa and 14.4 kPa at 50 % strain, respectively, which illustrated that the PVA-Lac@Cu/ZIFs hydrogel had a relatively high compression resistance. This result could be attributed to MOF nanocrystals anchoring onto hydrogel, which provided a premise for structural stability. Meanwhile, the maximum compression stress of both hydrogels reduced

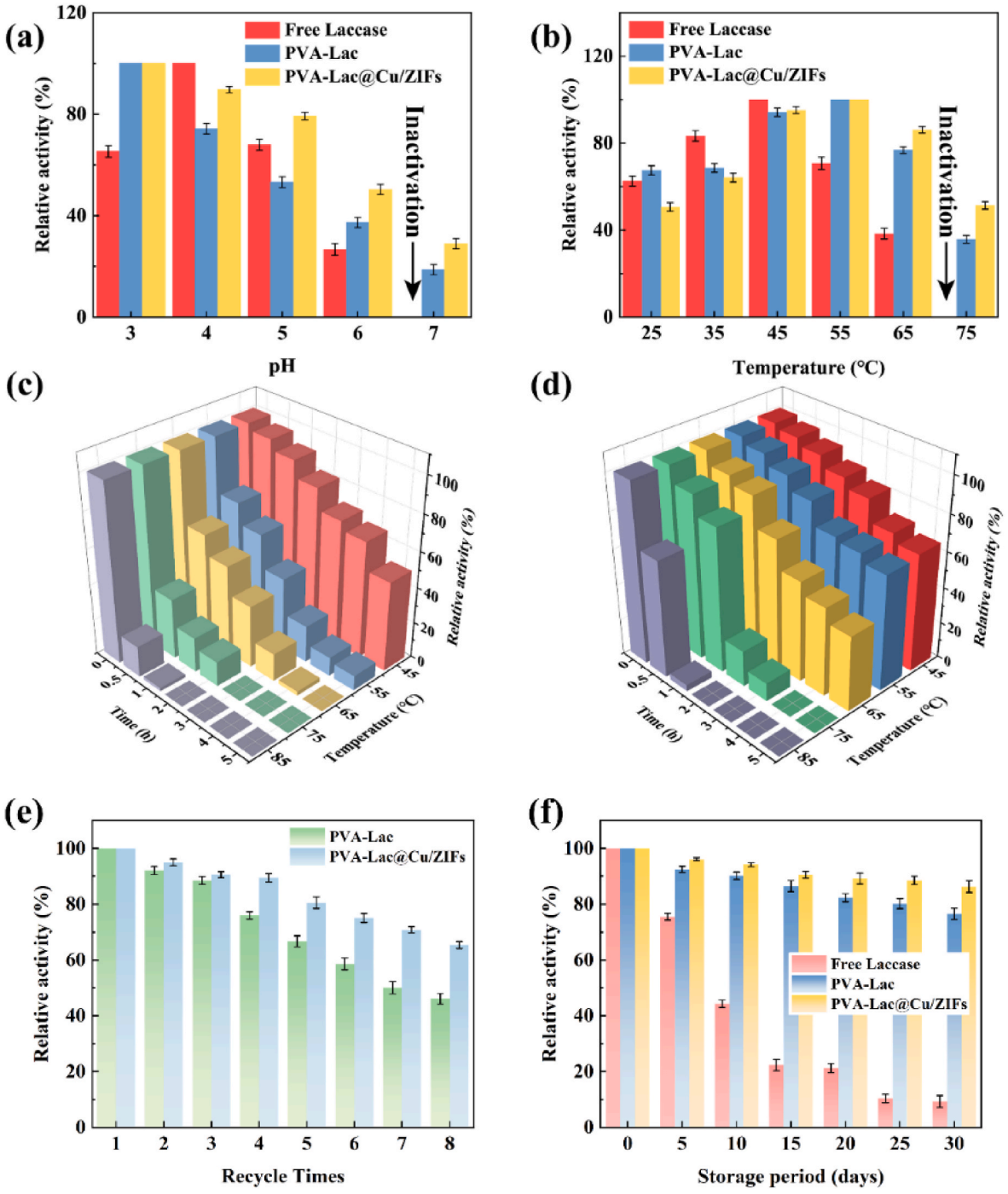

Fig. 3. Influence of pH (a) and temperature (b) on the activity of the free and immobilized laccase. Thermal stability of free laccase (c) and PVA-Lac@Cu/ZIFs hydrogel (d). Recyclability of PVA-Lac and PVA-Lac@Cu/ZIFs (e). Storage stability of free and immobilized laccase (f).

slightly, and the hydrogels exhibited good shape recovery ability and flexibility.

As shown in Fig. 2e, f, the thermal properties of the PVA-Lac and PVA-Lac@Cu/ZIFs were further investigated by TGA/DTG. The initial mass loss of both aerogels at around 200 °C could be attributed to the decomposition of laccase. The rapid huge weight loss at 200–300 °C was due to the removal of oxygen groups of polymer chains or the unreacted species trapped within the framework. The mass loss accounts for about 56 % and 52 %, respectively. For the PVA-Lac aerogels, the cracking and carbonization process of polymer chains occurred around 350–500 °C. When the temperature increased to 800 °C, only about 4 % of the original mass was left over. For PVA-Lac@Cu/ZIFs, the following weight loss step was observed at 400–500 °C due to the deformation of the framework (Liang et al., 2021a). The difference was that the PVA-Lac@Cu/ZIFs exhibited a slight weight loss when the temperature rose. The mass loss accounted for about only 11 %. Moreover, the internal structure of Cu-ZIF-90 was ordered and compact. PVA-Lac@Cu/ZIFs remained highly stable up to 350 °C and maintained about 21 % of the initial mass at 800 °C after the complete decomposition, indicating the PVA-Lac@Cu/ZIFs exhibited thermal stability.

3.2. Properties of the free and immobilized laccase

3.2.1. Optimal pH and temperature

The optimal pH of the free laccase, PVA-Lac and PVA-Lac@Cu/ZIFs was explored in the pH range from 3 to 7. As shown in Fig. 3a, the optimum pH of the free and immobilized laccase was 4 and 3, respectively. In our previous research, the optimum pH with the highest activity of Lac@Cu-ZIF-90 was 4.0 (Yang et al., 2023). The optimal pH for laccase activity was shifted after *in-situ* anchoring the Lac@Cu-ZIF-90 in PVA hydrogel. Generally, the charged support, which repelled or attracted the substrate, product, cofactor, and H, led to the changing microenvironment of the enzyme that could cause a shift in optimal pH. Owing to the acidic microenvironment created by acidic groups and the negative charge on the surface of the PVA, the solution must enhance the pH value to offset the influence of the microenvironment to maximize the activity of the immobilized enzyme (Chauhan et al., 2019). The hydroxide anion interrupted the internal electron transfer from *T1* to *T2/T3* copper sites in alkaline conditions. The activity of free and immobilization laccase was decreased. However, the immobilized laccase exhibited active stability with a broader pH range. When the pH of the environment reached an extreme of 7, the relative activity of both immobilized laccases was 18.7 % and 28.9 %, respectively. The free laccase was entirely inactive. Moreover, the encapsulated laccase with MOF nanocrystals would be confined to the change of conformation and microenvironment of laccase and thus maintain relatively higher activity.

The optimal free and immobilized laccase temperature was further investigated in the 25–75 °C temperature range. As shown in Fig. 3 b, the relative activity of free and immobilized laccase was increased with temperature from 25 to 45 °C. The optimum free and immobilized laccase temperature was 45 and 55 °C, respectively. Meanwhile, when the temperature rose to 75 °C, the free laccase was inactivated entirely, while the immobilized laccase exhibited a wider temperature tolerance. The relative activity of PVA-Lac and PVA-Lac@Cu/ZIFs was 37.5 % and 51.3 %, respectively. Compared with PVA-Lac, the PVA-Lac@Cu/ZIFs showed higher thermal stability. This result indicated that Lac@Cu-ZIF-90 could maintain a stable laccase conformation, further providing the spatial structure for laccase.

3.2.2. Thermal stability

Thermal stability was a critical parameter for evaluating the activity of laccase. Fig. 3c, d showed the relative activity of free laccase and PVA-Lac@Cu/ZIFs in a temperature range of 45–85 °C within 5 h. The enzyme structure gradually changed until completely inactivated under a high-temperature environment. Obviously, the free laccase was inactivated entirely after incubation for 3 h at 65 °C. Conversely, the thermal stability of PVA-Lac@Cu/ZIFs was significantly improved, and over 41.8 % of its initial activity was maintained. Furthermore, the free laccase was inactivated within 30 min when the temperature reached 85 °C, while the enzyme activity of PVA-Lac@Cu/ZIFs remained at 65.1 %.

Considering the above test analysis, the pH and thermal stability of immobilized laccase were significantly improved. The structural and tolerance stabilities of laccase immobilized on PVA-Cu-ZIF-90 hydrogel increased more than that of the PVA hydrogel. The porous structure and abundant unsaturated active site of Cu-ZIF-90 were conducive to maintaining the microenvironment of the enzyme. Therefore, the PVA-Lac@Cu/ZIFs exhibited great potential for further application.

3.2.3. Operational and storage stability of free and immobilized laccase

The operational stability of the immobilized laccase was evaluated via recycling experiments (Fig. 3e). Owing to the poor reusability and recyclability of the free enzyme, the practical application for laccase was hampered. Compared with free laccase, the PVA-Lac and PVA-Lac@Cu-ZIFs were effectively reused and separated from the reaction system. Remarkably, the residual activities of PVA-Lac and PVA-Lac@Cu-ZIFs still retained 46.1 % and 65.4 % of the initial activity after being recycled for 8 cycles, respectively. The laccase was disassociated or leached from the substrate during washing and reutilization. Meanwhile, the PVA-Lac@Cu-ZIFs exhibited the highest operational stability, illustrating that the Cu-ZIFs could protect the laccase against the influence of the external environment. In addition, the storage stability of free and immobilized laccase was explored. As shown in Fig. 3f, the immobilized laccase exhibited excellent long-term storage stability. The PVA-Lac@Cu-ZIFs retained nearly 86.3 % of initial activity after 30 days, while the free laccase had only 9.3 of initial activity. Owing to the MOFs provided sufficient space for laccase and significantly stabilized the conformational of protein. Based on the above research, the MOF-base hydrogel provided outstanding laccase protection and expanded the application range for laccase.

3.3. Preparation of PVA/ABTS-Lac and PVA/ABTS-Lac@Cu/ZIFs

The degradation performance of the co-immobilized LMS was assessed by decolorizing the typical structure pollutants: triphenylmethane dye-MG. The load capacity of ABTS on PVA-Lac and PVA-Lac@Cu/ZIFs hydrogels was investigated, as shown in Fig. 4 (a, b). When the concentration of ABTS was 2.0 mmol, the immobilized amount of ABTS on both hydrogels was around 1.9 mmol, and the highest removal rates of MG were 70.7 % and 69.4 %, respectively. With the increase of the ABTS concentration, the removal capacity of MG of hydrogels decreased. This phenomenon was due to the synthetic mediators with higher concentrations that could lead to laccase inactivation (Jeon et al., 2008). Therefore, the dosage of ABTS was selected as 2.0 mmol to prepare the co-immobilized LMS hydrogels. The UV–Vis absorption spectra of MG aqueous solution degraded by PVA/ABTS-Lac@Cu/ZIFs hydrogels within 5 h were shown in Fig. 4c. The two characteristic absorption peaks of MG were observed at 619 and 426 nm, and absorption intensity was decreased within 5 h. With the disappearance of the characteristic peaks, the absorption peak of new groups generated at 339 nm was found. This phenomenon showed that the chromophore of the dye was destroyed, and some of the MG was degraded to some small molecules.

3.4. Decolorization of MG

The effects of initial dye concentration, reaction temperature and initial pH on MG degradation were investigated to evaluate the catalytic ability of co-immobilization LMS comprehensively. In addition, to investigate the degradation efficiency of both two hydrogels, the degradation kinetics curves of MG under different conditions were

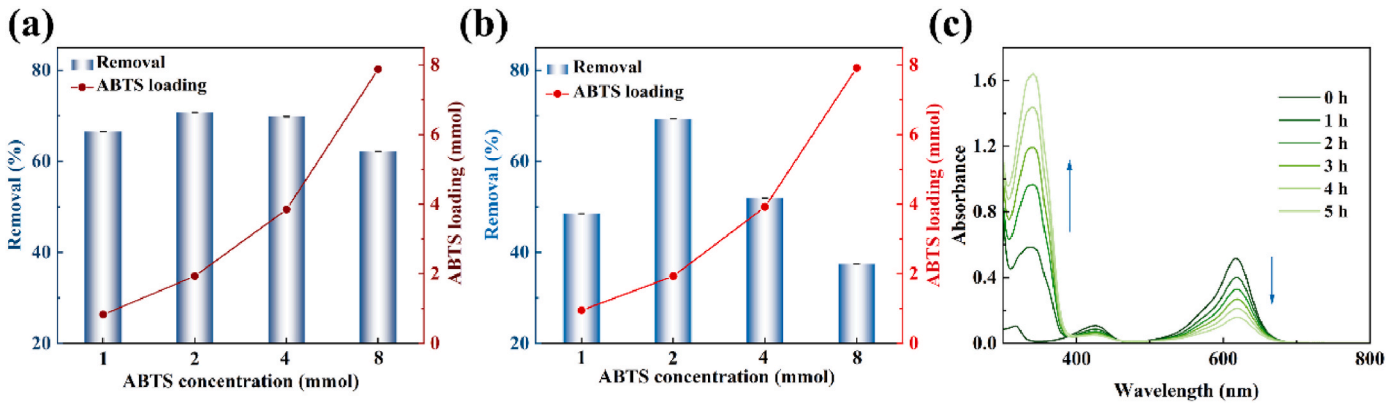

Fig. 4. Effect of the ABTS dosage on immobilized ABTS of PVA-Lac (a) and PVA-Lac@Cu/ZIFs (b) hydrogel. (c) Changes of the characteristic absorption after degradation by PVA/ABTS-Lac@Cu/ZIFs.

calculated. The degradation kinetics models were expressed as follows:

$$\ln\left(\frac{C_t}{C_0}\right) = -k_1 t$$

C_0 and C_t were the initial equilibrium concentration and the actual concentration of MG at reaction time t. The k_1 (h^{-1}) was the rate constant of pseudo-first-order kinetics.

As shown in Fig. 5 (a, g), the removal rate of MG by PVA/ABTS-Lac and PVA/ABTS-Lac@Cu/ZIFs reduced as the MG concentration increased from 10 to 90 mg/L. When the concentration of MG was 10 mg/L, both hydrogels showed a maximum degradation rate of 88.3 % and 89.7 %, respectively. The co-immobilization LMS exhibited the highest reaction rate constants of 0.476 and 0.442, respectively. With the increasing MG concentration, the degradation rate and reaction rate constants of PVA/ABTS-Lac and PVA/ABTS-Lac@Cu/ZIFs were significantly decreased. When the concentration of MG increased by 50 mg/L, the degradation rate showed a significant decrease. However, over 50 % of MG was degraded, and the k value decreased to 0.165 and 0.182, respectively (Fig. 5 d, j). With the MG concentration further increased, the degradation rates and reaction rate constants of PVA/ABTS-Lac and PVA/ABTS-Lac@Cu/ZIFs significantly decreased. This result indicated the high concentration of MG could compete with the active sites of laccase and inhibit the interaction between the substrate and laccase.

The critical reaction parameters for MG degradation efficiency were further investigated to optimize the degradation condition, including reaction temperature and pH. The PVA/ABTS-Lac and PVA/ABTS-Lac@Cu/ZIFs exhibited a high degradation activity over a wide temperature of 35–55 °C. As shown in Fig. 5 (b, h), the degradation performance of both two hydrogels improved with the temperature increase from 35 to 55 °C. The degradation rates were improved to 80.9 % and 87.1 %, respectively. Furthermore, the best catalytic rate and the highest reaction rate constants were obtained when the reaction temperature was raised to 55 °C. These results could be attributed to the high temperature driving MG molecules to move positively. Moreover, the degradation rate of PVA/ABTS-Lac@Cu/ZIFs was further improved to 90.8 %, and the highest reaction rate constants of 0.699 were obtained (Fig. 5 e, k). These results indicated that MOF nanocrystals and PVA hydrogels provided an advantageous environment for laccase, and the Cu-ZIF-90 further acted as a shield to relieve the conformation change of the enzyme.

The initial pH cold impacted the active sites of laccase and internal electron transfer, meanwhile changing the enzyme microenvironment. Therefore, the effectiveness of the initial pH for the degradation system was further investigated. As shown in Fig. 5 (c, i), the degradation rate and reaction rate constants of the co-immobilization LMS were markedly increased in acid environments. The PVA/ABTS-Lac and PVA/ABTS-Lac@Cu/ZIFs exhibited the maximum reaction rate constants at pH 3.0, as shown in Fig. 5 (f, i). The degradation rates for MG of both hydrogels approached 100 % within 4 h and showed a degradation rate of 0.846 and 0.876, respectively. Compared with the PVA/ABTS-Lac hydrogel, the enhancement of degradation efficiency of PVA/ABTS-Lac@Cu/ZIFs was more significant. The Lac@Cu-ZIF-90 used the laccase active center, Cu^{2+}, as the component constructs the MOFs, which could accelerate the transfer of electrons between the laccase active centers in the acid environment, further increasing the degradation efficiency. Based on the above results, the MOF nanocrystals provided the protective layer for laccase, increasing the electron transfer between the laccase and substrates.

Except for the temperature and initial pH of reaction parameters, the effects of various cations on the degradation process for MG were evaluated. The degradation kinetics curves of MG in the presence of various cations were calculated. As shown in Fig. 6 (a, b), the coexistence of metal ions inhibited the degradation process for MG by PVA/ABTS-Lac@Cu/ZIFs in various degrees. On the one hand, the different metal ions could affect the solubility and swelling of PVA polymer chains(Wu et al., 2021). The cationic dyes and coexisting metal cations were existing competitive adsorption with polymer chains, leading to the interaction between the MG molecules and PVA polymer chains decreasing slightly. On the other hand, the metal ions bound with the active site of laccase, leading to the blockage of the electron transfer system. Therefore, the degradation efficiency of PVA/ABTS-Lac@Cu/ZIFs was decreased within the coexistence of metal ions. Although the degradation efficiency of PVA/ABTS-Lac@Cu/ZIFs was reduced, over 50 % of MG was degraded within 5 h. It illustrated that the PVA/ABTS-Lac@Cu/ZIFs hydrogel had potential applications in practical water treatment.

The reusability of co-immobilized LMS was one of the critical parameters in practical application. The PVA/ABTS-Lac and PVA/ABTS-Lac@Cu/ZIFs hydrogels were used for five consecutive degradation cycles to degrade 30 mg/L MG. As shown in Fig. 6c, the degradation rate of PVA/ABTS-Lac@Cu/ZIFs hydrogel for MG was 80.7 % in the third cycle. The degradation rate was only reduced by 12 % compared with the first cycle. However, the degradation rate gradually decreased with the increase of degradation cycles. The degradation rate for MG decreased to 69.4 % in the fifth cycle. The reusability of PVA/ABTS-Lac was relatively poor compared with PVA/ABTS-Lac@Cu/ZIFs. The degradation rate for MG decreased to 50.9 % after five cycles. This result illuminated that the *in-situ* synthesis of MOF nanoparticles in PVA hydrogels exhibited significant co-immobilization effects, the laccase was encapsulated in MOFs, and ABTS crosslinked on the surface of hydrogel, leading to the high reusability. However, the progressive leaching of enzymes from MOFs and the disassociation of ABTS on the surface of hydrogel reduced the degradation rate.

Different dye solutions were used to simulate the targeted textile

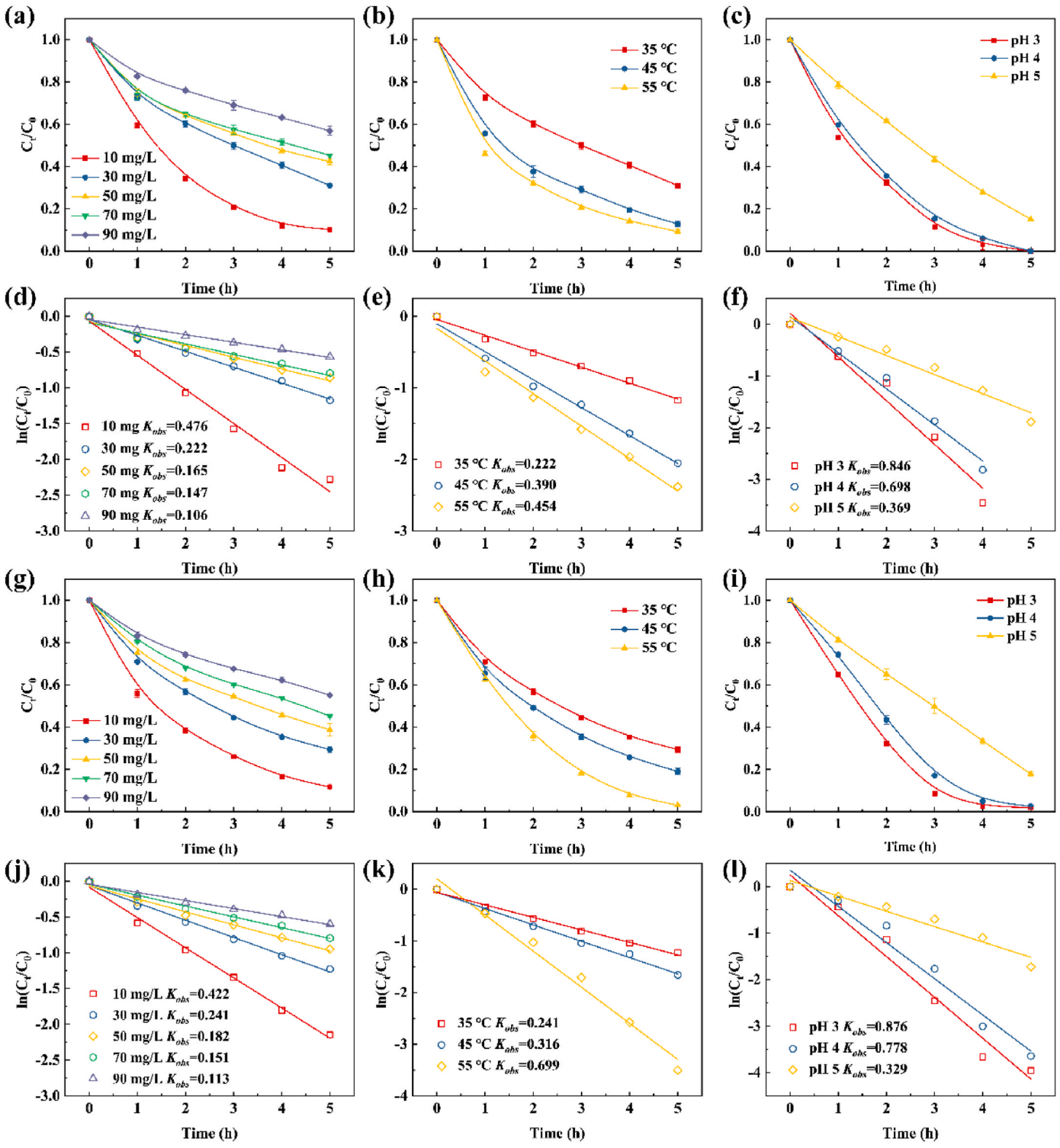

Fig. 5. MG degradation efficiency and kinetics curves by PVA/ABTS-Lac (a, d) and PVA/ABTS-Lac@Cu/ZIFs (g, j) with diverse initial dye concentrations. The effect of different environmental parameters on degradation efficiency and degradation kinetics curves of MG, (b, e and h, k) reaction temperature and (c, f and i, l) initial pH.

wastewater for decolorization to demonstrate the potential of the PVA/ABTS-Lac@Cu/ZIFs hydrogels in wastewater treatment. The decolorization of the dye solution was evaluated using acid orange 7 (AO), congo red (CR), and reactive blue 19 (RB) with the initial dye concentration (50 mg/L) within 5 h, respectively. As shown in Fig. 6d, the removal of AO, CR and RB for co-immobilized LMS was 85.3 %, 98.1 % and 80.3 %, respectively. The redox potential of the mediator and functional group of dye molecules determined the reaction efficiency of LMS (Espina et al., 2021; Lou et al., 2023). The degradation of the azo dye, AO, and CR occurred through the asymmetric cleavage of the azo bond (Li et al., 2022a). For a more complex structure of anthraquinone dyes, RB, the PVA/ABTS-Lac@Cu/ZIFs hydrogels exhibited a relatively poor decolorization effect.

In addition, the related studies on MG degradation by laccase or LMS

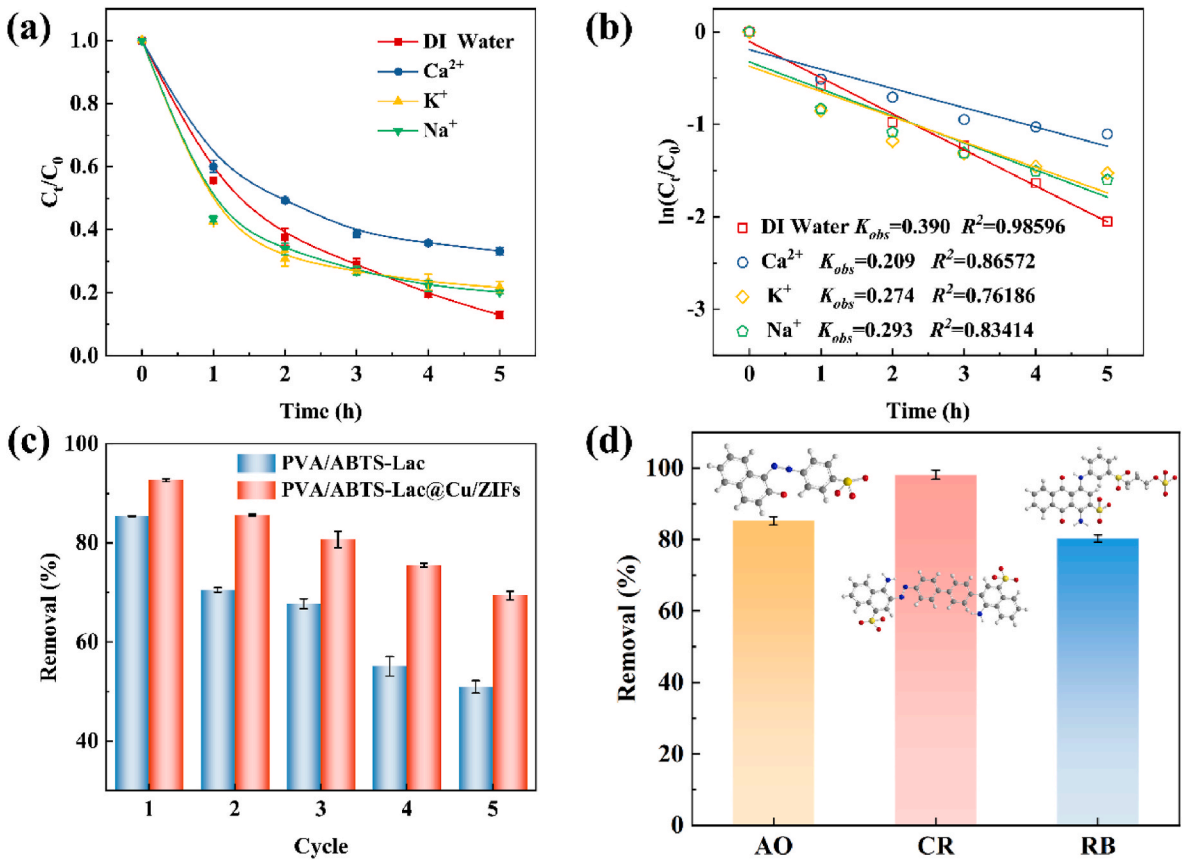

Fig. 6. (a) Effects of various cations on the decolorization of MG with PVA/ABTS-Lac@Cu/ZIFs hydrogel. (b) The pseudo-first-order kinetics for MG. (c) Reusability of PVA/ABTS-Lac and PVA/ABTS-Lac@Cu/ZIFs hydrogels for MG degradation.

in recent years were summarized, as shown in Table S1. Compared with other free or co-immobilized LMS, the PVA/ABTS-Lac and PVA/ABTS-Lac@Cu/ZIFs hydrogels prepared in this study exhibited a better performance in degradation.

3.5. Degradation pathway and mechanism

The liquid chromatograph mass spectrometer (LC-MS) technique was used to identify the possible transformation intermediates and final products to elucidate the degradation pathway for MG by the PVA/

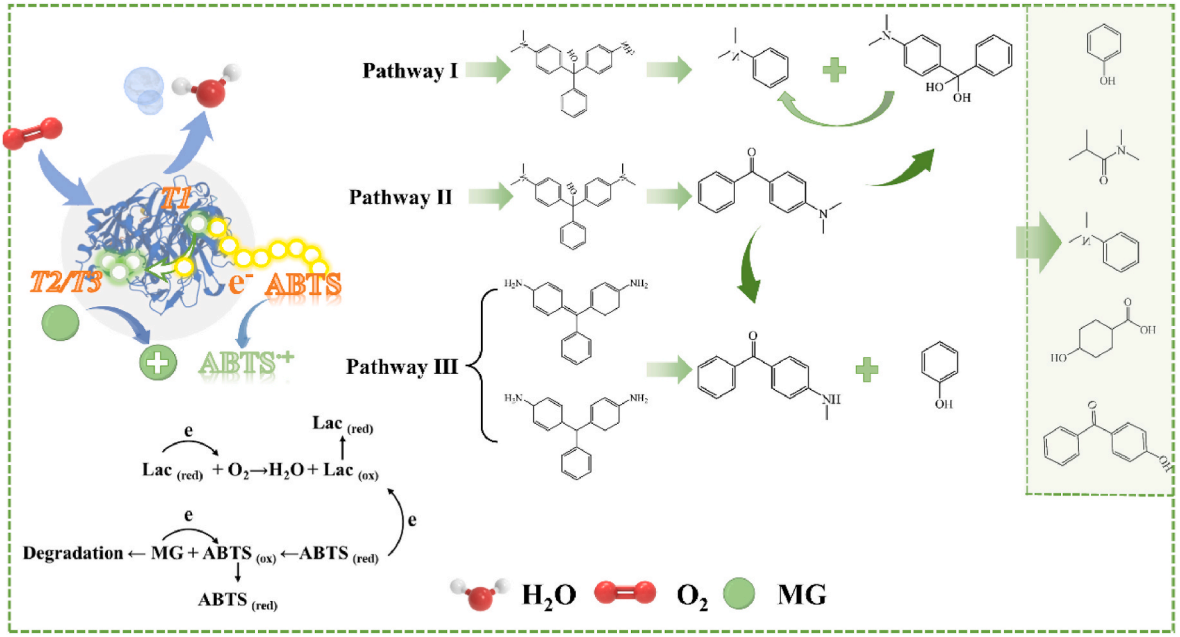

Fig. 7. Possible degradation pathway of MG by PVA/ABTS-Lac@Cu/ZIFs system and the reaction mechanism for MG degradation by co-immobilized LMS.

ABTS-Lac@Cu/ZIFs hydrogel. The corresponding mass spectra were illustrated in Fig. S4. According to the LC-MS results, the possible degradation pathway was shown in Fig. 7. The MG was divided into demethylation and hydroxylation and decomposed into $m/z = 318$, 347 and $m/z = 274$, respectively. For pathway I, fragments with $m/z = 243$ and $m/z = 120$ were further produced by the cleavage of carbon atoms (Mao et al., 2021). Additionally, the intermediates with $m/z = 243$ were degraded via further oxidative cleavage to $m/z = 120$ for further degradation. Regarding pathway II, the central carbon atom of products with $m/z = 347$ was further breaking. The cleavage of the central carbon atom and demethylation produced the productions with m/z = 226. Subsequently, the intermediates with $m/z = 226$ were hydroxylated and demethylated to form the $m/z = 243$ and $m/z = 212$, respectively. The productions with $m/z = 274$ could also be converted into $m/z = 212$ in the pathway III. The intermediates with $m/z = 212$ and $m/z = 95$ were formed via cleavage of the central carbon atom of the C–C bond (Cheng et al., 2021; Wang et al., 2022c). Finally, these productions could be further decomposed into other smaller molecules via eradicating benzene ring, N-demethylation and oxidation, with significantly reduced ecotoxicity.

Based on the LC-MS analysis of the possible transformation intermediates and final products, the degradation mechanism of co-immobilized laccase and ABTS (Wang et al., 2022b, 2023). Firstly, the mediator ABTS immobilized on the hydrogel was gradually oxidized at the *T1* site in laccase, and the electrons were transferred to the trinuclear *T2/T3* copper cluster. The mediator ABTS was oxidized to the $ABTS^{\cdot+}$ with high redox potential. Then, the $ABTS^{\cdot+}$ further oxidized MG molecules via electron transfer from MG molecules. The MG molecules lose electrons and form an electron-deficient center, and the carbon atoms cleavage to form intermediate products. Finally, these products were further decomposed into other smaller molecules, and the efficiency of electron transfer from ABTS to laccase dominates the activity of LMS.

4. Conclusion

In summary, the biocatalyst PVA/ABTS-Lac@Cu/ZIFs with high catalytic activity and stability have been prepared by co-immobilizing laccase and ABTS on the MOF/hydrogel via a facile freeze-thaw cycle method. The MOF/hydrogel exhibited an excellent protective effect on laccase in various interfering environments. The PVA-Lac@Cu/ZIFs hydrogel could remain about 50.3 % of their initial activity at pH 6, while the free laccase was almost inactivated at the same condition. Moreover, the PVA-Lac@Cu/ZIFs hydrogel demonstrated high decoloration efficiency for MG dyes (practically 100 %) within 4 h. More importantly, the laccase and ABTS could be recycled synchronously and reused for more cycles. After five cycles, the biocatalyst exhibited considerable catalytic activity for MG degradation. The successful reuse of laccase and mediator offered a solution for the potential of water treatment, and the MOF/hydrogel as a protective layer to protect the laccase against the industrial environment provides the possibility of further developing biocomposite for industrial applications.

CRediT authorship contribution statement

Xue Yang: Writing – original draft, Visualization, Methodology, Formal analysis, Data curation, Conceptualization. **Xinyi Chen:** Writing – review & editing, Supervision, Conceptualization. **Hongbo Wang:** Supervision, Resources, Conceptualization. **Artur Cavaco-Paulo:** Writing – review & editing, Supervision. **Jing Su:** Conceptualization, Writing – review & editing, Visualization, Validation, Supervision, Resources.

Declaration of competing interest

The authors declare that they have no known competing financial interests or personal relationships that could have appeared to influence the work reported in this paper.

Data availability

Data will be made available on request.

Acknowledgments

We thank the financial support from the National Natural Science Foundation of China (Grant No. 52003108), the China Postdoctoral Science Foundation funded project (2022M721359), and the Post-graduate Research & Practice Innovation Program of Jiangsu Province (KYCX23_2476).

Appendix A. Supplementary data

Supplementary data to this article can be found online at https://doi.org/10.1016/j.jenvman.2024.120114.

References

Ahmadian, M., Derakhshankhah, H., Jaymand, M., 2023. Recent advances in adsorption of environmental pollutants using metal–organic frameworks-based hydrogels. Int. J. Biol. Macromol. 231, 123333.
Cañas, A.I., Camarero, S., 2010. Laccases and their natural mediators: Biotechnological tools for sustainable eco-friendly processes. Biotechnol. Adv. 28, 694–705.
Chandio, I., Ai, Y., Wu, L., Liang, Q., 2024. Recent progress in MOFs-based nanozymes for biosensing. Nano 17, 39–64.
Chauhan, P.S., Kumarasamy, M., Sosnik, A., Danino, D., 2019. Enhanced Thermostability and Anticancer activity in Breast cancer cells of laccase immobilized on pluronic-stabilized nanoparticles. ACS Appl. Mater. Interfaces 11, 39436–39448.
Chen, W.-T., Zeng, L., Li, P., Liu, Y., Huang, J.-L., Guo, H., Rao, P., Li, W.-H., 2023. Convenient hydrogel adhesion with crystalline zones. J. Ind. Eng. Chem. 117, 103–108.
Cheng, C.-M., Patel, A.K., Singhania, R.R., Tsai, C.-H., Chen, S.-Y., Chen, C.-W., Dong, C. D., 2021. Heterologous expression of bacterial CotA-laccase, characterization and its application for biodegradation of malachite green. Bioresour. Technol. 340, 125708.
Dai, L., Lou, J., Baek, N.-w., Zhang, X., Yuan, J., Xu, J., Fan, X., 2022. A rapid way of preparing switchable bacteria-killing and bacteria-releasing cellulosic material with anti-bacteria adhesion capability. Cellulose 29, 5305–5323.
Dai, L., Yuan, J., Xu, J., Lou, J., Fan, X., 2023. Switchable bacteria-killing and bacteria-releasing surface fabricated from regenerable PNIPAM-based N-halamine cotton fabrics. Prog. Org. Coating 182, 107650.
Dong, C.-D., Tiwari, A., Anisha, G.S., Chen, C.-W., Singh, A., Haldar, D., Patel, A.K., Singhania, R.R., 2023. Laccase: a potential biocatalyst for pollutant degradation. Environ. Pollut. 319, 120999.
Drout, R.J., Robison, L., Farha, O.K., 2019. Catalytic applications of enzymes encapsulated in metal–organic frameworks. Coord. Chem. Rev. 381, 151–160.
Duman, O., Diker, C.Ö., Uğurlu, H., Tunç, S., 2022a. Highly hydrophobic and superoleophilic agar/PVA aerogels for selective removal of oily substances from water. Carbohydr. Polym. 286, 119275.
Duman, O., Polat, T.G., Tunç, S., 2022b. Development of poly(vinyl alcohol)/β-cyclodextrin/P(MVE-MA) composite nanofibers as effective and selective adsorbent and filtration material for the removal and separation of cationic dyes from water. J. Environ. Manag. 322, 116130.
Duman, O., Uğurlu, H., Diker, C.Ö., Tunç, S., 2022c. Fabrication of highly hydrophobic or superhydrophobic electrospun PVA and agar/PVA membrane materials for efficient and selective oil/water separation. J. Environ. Chem. Eng. 10, 107405.
Espina, G., Cáceres-Moreno, P., Mejías-Navarrete, G., Ji, M., Sun, J., Blamey, J.M., 2021. A novel and highly active recombinant spore-coat bacterial laccase, able to rapidly biodecolorize azo, triarylmethane and anthraquinonic dyestuffs. Int. J. Biol. Macromol. 170, 298–306.
Hsu, P.-H., Chang, C.-C., Wang, T.-H., Lam, P.K., Wei, M.-Y., Chen, C.-T., Chen, C.-Y., Chou, L.-Y., Shieh, F.-K., 2021. Rapid fabrication of biocomposites by encapsulating enzymes into Zn-MOF-74 via a mild water-based approach. ACS Appl. Mater. Interfaces 13, 52014–52022.
Hu, J., Wu, Y., Yang, Q., Zhou, Q., Hui, L., Liu, Z., Xu, F., Ding, D., 2022. One-pot freezing-thawing preparation of cellulose nanofibrils reinforced polyvinyl alcohol based ionic hydrogel strain sensor for human motion monitoring. Carbohydr. Polym. 275, 118697.
Hu, Y., Dai, L., Liu, D., Du, W., Wang, Y., 2018. Progress & prospect of metal-organic frameworks (MOFs) for enzyme immobilization (enzyme/MOFs). Renew. Sustain. Energy Rev. 91, 793–801.
Hwang, E.T., Lee, S., 2019. Multienzymatic cascade reactions via enzyme complex by immobilization. ACS Catal. 9, 4402–4425.
Idriss, H., 2021. On the wrong assignment of the XPS O1s signal at 531–532 eV attributed to oxygen vacancies in photo- and electro-catalysts for water splitting and other materials applications. Surf. Sci. 712, 121894.

Jeon, J.-R., Murugesan, K., Kim, Y.-M., Kim, E.-J., Chang, Y.-S., 2008. Synergistic effect of laccase mediators on pentachlorophenol removal by Ganoderma lucidum laccase. Appl. Microbiol. Biotechnol. 81, 783–790.

Li, W., Wang, Z., Li, Y., Ghasemi, J.B., Li, J., Zhang, G., 2022a. Visible-NIR light-responsive 0D/2D CQDs/Sb2WO6 nanosheets with enhanced photocatalytic degradation performance of RhB: unveiling the dual roles of CQDs and mechanism study. J. Hazard Mater. 424, 127595.

Li, X., Wu, Z., Tao, X., Li, R., Tian, D., Liu, X., 2022b. Gentle one-step co-precipitation to synthesize bimetallic CoCu-MOF immobilized laccase for boosting enzyme stability and Congo red removal. J. Hazard Mater. 438, 129525.

Liang, W., Wang, B., Cheng, J., Xiao, D., Xie, Z., Zhao, J., 2021a. 3D, eco-friendly metal-organic frameworks@carbon nanotube aerogels composite materials for removal of pesticides in water. J. Hazard Mater. 401, 123718.

Liang, W., Wied, P., Carraro, F., Sumby, C.J., Nidetzky, B., Tsung, C.-K., Falcaro, P., Doonan, C.J., 2021b. Metal–organic framework-based enzyme biocomposites. Chem. Rev. 121, 1077–1129.

Liu, D., Cao, Y., Jiang, P., Wang, Y., Lu, Y., Ji, Z., Wang, X., Liu, W., 2023. Tough, transparent, and slippery PVA hydrogel led by syneresis. Small 19, 2206819.

Liu, Y.-R., Chen, Y.-Y., Zhuang, Q., Li, G., 2022. Recent advances in MOFs-based proton exchange membranes. Coord. Chem. Rev. 471, 214740.

Lou, X., Zhi, F., Sun, X., Wang, F., Hou, X., Lv, C., Hu, Q., 2023. Construction of co-immobilized laccase and mediator based on MOFs membrane for enhancing organic pollutants removal. Chem. Eng. J. 451, 138080.

Luo, Q., Yan, X., Lu, J., Huang, Q., 2018. Perfluorooctanesulfonate degrades in a laccase-mediator system. Environ. Sci. Technol. 52, 10617–10626.

Luo, X., Zhu, L., Wang, Y.-C., Li, J., Nie, J., Wang, Z.L., 2021. A flexible multifunctional triboelectric nanogenerator based on MXene/PVA hydrogel. Adv. Funct. Mater. 31, 2104928.

Mao, G., Wang, F., Wang, J., Chen, P., Zhang, X., Zhang, H., Wang, Z., Song, A., 2021. A sustainable approach for degradation and detoxification of malachite green by an engineered polyphenol oxidase at high temperature. J. Clean. Prod. 328, 129437.

Peng, J., Wu, E., Lou, X., Deng, Q., Hou, X., Lv, C., Hu, Q., 2021. Anthraquinone removal by a metal-organic framework/polyvinyl alcohol cryogel-immobilized laccase: effect and mechanism exploration. Chem. Eng. J. 418, 129473.

Rahman, M.T., Rahman, M.S., Kumar, H., Kim, K., Kim, S., 2023. Metal-organic framework reinforced highly stretchable and durable conductive hydrogel-based triboelectric nanogenerator for biomotion sensing and wearable human-machine interfaces. Adv. Funct. Mater. 33, 2303471.

Su, J., Noro, J., Fu, J., Wang, Q., Silva, C., Cavaco-Paulo, A., 2018. Enzymatic polymerization of catechol under high-pressure homogenization for the green coloration of textiles. J. Clean. Prod. 202, 792–798.

Wang, L., Xu, H., Gao, J., Yao, J., Zhang, Q., 2019. Recent progress in metal-organic frameworks-based hydrogels and aerogels and their applications. Coord. Chem. Rev. 398, 213016.

Wang, M., Zhou, H., Du, H., Chen, L., Zhao, G., Liu, H., Jin, X., Chen, W., Ma, A., 2022a. A cyclic freezing-thawing approach to layered Janus hydrogel tapes with single-sided adhesiveness for wearable strain sensors. Chem. Eng. J. 446, 137163.

Wang, X., Ren, Y., Li, Y., Zhang, G., 2022b. Fabrication of 1D/2D BiPO4/g-C3N4 heterostructured photocatalyst with enhanced photocatalytic efficiency for NO removal. Chemosphere 287, 132098.

Wang, Z., Li, W., Wang, J., Li, Y., Zhang, G., 2023. Novel Z-scheme AgI/Sb2WO6 heterostructure for efficient photocatalytic degradation of organic pollutants under visible light: interfacial electron transfer pathway, DFT calculation and mechanism unveiling. Chemosphere 311, 137000.

Wang, Z., Ren, D., Zhang, X., Zhang, S., Chen, W., 2022c. Adsorption-degradation of malachite green using alkali-modified biochar immobilized laccase under multi-methods. Adv. Powder Technol. 33, 103821.

Wu, S., Hua, M., Alsaid, Y., Du, Y., Ma, Y., Zhao, Y., Lo, C.-Y., Wang, C., Wu, D., Yao, B., Strzalka, J., Zhou, H., Zhu, X., He, X., 2021. Poly(vinyl alcohol) hydrogels with broad-range tunable mechanical properties via the hofmeister effect. Adv. Mater. 33, 2007829.

Wu, S., Zhu, C., He, Z., Xue, H., Fan, Q., Song, Y., Francisco, J.S., Zeng, X.C., Wang, J., 2017. Ion-specific ice recrystallization provides a facile approach for the fabrication of porous materials. Nat. Commun. 8, 15154.

Wu, W., Liu, J., Lin, X., He, Z., Zhang, H., Ji, L., Gong, P., Zhou, F., Liu, W., 2023. Dual-functional MOFs-based hybrid microgel advances aqueous lubrication and anti-inflammation. J. Colloid Interface Sci. 644, 200–210.

Yang, X., Zhao, J., Cavaco-Paulo, A., Su, J., Wang, H., 2023. Encapsulated laccase in bimetallic Cu/Zn ZIFs as stable and reusable biocatalyst for decolorization of dye wastewater. Int. J. Biol. Macromol. 233, 123410.

Yao, C., Xia, W., Dou, M., Du, Y., Wu, J., 2022. Oxidative degradation of UV-irradiated polyethylene by laccase-mediator system. J. Hazard Mater. 440, 129709.

Zdarta, J., Jankowska, K., Bachosz, K., Degórska, O., Kaźmierczak, K., Nguyen, L.N., Nghiem, L.D., Jesionowski, T., 2021. Enhanced wastewater treatment by immobilized enzymes. Current Pollution Reports 7, 167–179.

Zhang, H., Hay, A.G., 2020. Magnetic biochar derived from biosolids via hydrothermal carbonization: enzyme immobilization, immobilized-enzyme kinetics, environmental toxicity. J. Hazard Mater. 384, 121272.

Zhang, R., Wang, L., Han, J., Wu, J., Li, C., Ni, L., Wang, Y., 2020. Improving laccase activity and stability by HKUST-1 with cofactor via one-pot encapsulation and its application for degradation of bisphenol A. J. Hazard Mater. 383, 121130.

Zhao, Z., Shehzad, M.A., Wu, B., Wang, X., Yasmin, A., Zhu, Y., Wang, X., He, Y., Ge, L., Li, X., Xu, T., 2021. Spray-deposited thin-film composite MOFs membranes for dyes removal. J. Membr. Sci. 635, 119475.

Zhou, W., Zhang, W., Cai, Y., 2021. Laccase immobilization for water purification: a comprehensive review. Chem. Eng. J. 403, 126272.